Pergamon

Int. J. Solids Structures Vol. 32, No. 6/7, pp. 739–765, 1995

0020–7683/95 $9.50 + .00

0020–7683(94)00158–8

PREDICTION OF COMPRESSIVE STRENGTH AND KINK BANDS IN COMPOSITES USING A WORK POTENTIAL

R. A. SCHAPERY
Department of Aerospace Engineering and Engineering Mechanics, The University of Texas, Austin, TX 78712-1085, U.S.A.

(*Received* 1 *February* 1993; *in revised form* 26 *May* 1994)

Abstract—A recently developed method of characterizing nonlinear, inelastic behavior of composites is described and then used to provide constitutive equations for use in the compressive strength problem of unidirectional fiber composites. This constitutive theory, which is based on a work potential, appears to be valid for the strain state and levels of strain needed to predict kink band angles and compressive strength. A one-dimensional deformation model of fiber waviness growth is then described and used to make a case that a band of wavy fibers initiates a kink band when local matrix cracking occurs and the axial stress equals or exceeds the predicted critical stress for local buckling. This requirement of matrix cracking serves to define the kink band angle. For multiaxial stresses this angle and the compressive strength depend on all components of the overall or average stresses; the multiaxial state of stress may arise from external loading or from ply-to-ply interactions in a multi-directional laminate. Equations are developed for predicting the behavior for general in-plane loading and arbitrarily large geometric nonlinearities when the failure mechanism is microbuckling. A geometrically approximate, analytical solution is also developed. Results for several cases are given in order to illustrate the predicted behavior and to show that the predictions are consistent with experimental observations.

1. INTRODUCTION

Microbuckling appears to be the primary compressive strength limiting mechanism in unidirectional fiber-reinforced plastics subjected to an axial load in the fiber direction. Over the past three decades, linear elasticity theory of varying degrees of complexity has been used in many studies of failure by fiber buckling. For the high levels of fiber volume fraction used in structural composites, Rosen (1965) showed in a linear, two-dimensional bifurcation analysis that the critical deformation mode is one in which the wavelength is long compared to fiber diameter, and locally it involves simple shearing. The buckling stress was predicted to be approximately the principal composite shear modulus G_{12}. However, measured strengths are commonly one-third to one-sixth of this modulus (Budiansky and Fleck, 1993). Linear elasticity studies which have accounted for free surface effects (Waas *et al.* 1990) and approximate three-dimensional effects (Greszczuk, 1975) did not succeed in predicting strengths which are lower than G_{12}.

Post failure inspection of test specimens reveals kink bands, such as those illustrated in Fig. 1. The circular, cylindrical specimen in Fig. 1(b) was in a steel tube (whose inner surface was at the left edge where the kink bands meet) which globally stabilized the specimen and lead to multiple kink bands, two of which are illustrated in this section view. This mode of failure motivated Argon (1972) and Budiansky (1983) to develop simple kink band models which predict realistic compressive strengths. For a narrow band of initially misaligned, inextensible fibers which is normal to the average fiber direction, as in Fig. 2 with $\beta = 0$, elementary equilibrium considerations give the equation for axial stress,

$$\sigma_1 = \frac{\tau_{12}}{\phi_0 + \gamma_{12}}$$

where τ_{12} and γ_{12} are the shear stress and strain, respectively, and ϕ_0 is the initial, small misalignment angle. If we write $\tau_{12} = G_{12}\gamma_{12}$ and use for G_{12} a typical, decreasing function of shear strain based on experiments and a representative value of $\phi_0 = 2^\circ$, this equation

predicts a realistic maximum stress (i.e. compressive strength) which is significantly less than Rosen's result of $G_{12}(0)$. Argon (1972), assuming rigid–perfectly plastic behavior, estimated the compressive strength as $\sigma_c = \tau_y/\phi_0$, where τ_y is the yield strength, while Budiansky (1983) included the effect of shear strain at yield, $\gamma_{12} = \gamma_y$, in an elastic–perfectly plastic composite. Budiansky further showed that when $\beta > 0$, the compressive strength is increased, thus leading one to expect to find $\beta = 0$ in failed specimens. Inasmuch as measured values of kink band angles are significantly greater than 0°, sometimes exceeding 30° (Hahn and Williams, 1986), these elementary analyses of long misalignment bands fall short of capturing all of the important physics of the microbuckling problem.

In an effort to introduce more realism in the analysis, Kyriakides *et al.* (1995) developed a two-dimensional (plane strain) finite element model for predicting growth of fiber waviness, starting with various initial wave patterns, up to and beyond the maximum axial stress; the composite microgeometry was represented by distributed layers of fiber and matrix material. A kink band geometry was predicted to develop through a strain localization process. The initial states of fiber waviness used by these authors consisted of sinusoidal waves in the mean fiber direction with constant amplitude and with variable amplitude variations in the fiber direction or normal to the fibers. The effect of variable matrix volume fraction was also studied. The largest predicted deformation band angles (which were within their experimentally observed range of 11°–16° for kink bands) were for the case in which the initial wave amplitude decayed symmetrically in the direction normal to the mean fiber direction; the largest amplitude was in the center of specimen. Compressive strength and band width at the time of fiber breakage were shown to be in reasonable agreement with experimental results. The kink band width, as set by the spacing between the pair of breaks in each fiber, was predicted to scale with the microstructure scale, with a fiber bending failure criterion leading to a kink width on the order of 25 fiber diameters (which is the spacing of the local maximum moments); comparable widths were predicted by Fleck *et al.* (1993) using a one-dimensional continuum analysis with couple stresses. These width predictions are for the commonly observed, very long fiber misalignment wavelengths compared to the microstructure scale. Shorter wavelengths (in the fiber direction) were predicted to result in slightly narrower band widths. In a few cases, Daniel (1993, 1994) observed band widths of only 4–7 fiber diameters in a carbon/epoxy (IM6G/3501-6) composite; these narrow bands, which may be associated with short wavelength initial imperfections, have a kink band angle of approximately 30°, while his more commonly observed widths of 16–20 diameters have kink band angles of approximately 20°, as in Fig. 1(a).

To date, apart from the work of Kyriakides *et al.* (1995), very little progress has been made on predicting realistic kink band angles. In an early study, Budiansky (1983) estimated the angle to be in the range of 10°–35°. His prediction was based on the elastic deformations which result from local, irregular edge imperfections. This deformation is in bands whose orientations fall in this range; they were interpreted as initial imperfections for the microbuckling problem.

The present paper is concerned, in part, with predicting the kink band angle by using a criterion which is different from those in these two studies. Whether a kink band starts from a well-defined *initial* band of wavy fibers or from a deformation induced band, the problem is to determine which band orientation is the most likely one to be a source of kink bands. Inasmuch as existing analyses show that the maximum axial stress which can be supported by a long band of misaligned fibers depends (somewhat) on β, the prediction also is concerned with the compressive strength due to microbuckling. The initial imperfection is assumed here to be characterized by wavelengths that are long compared to the microstructure, which permits the use of a constitutive model of a *homogeneous* orthotropic material. Although the kink band width scales with the microstructure, the analysis in this paper indicates that the kink band angle is set by matrix microcracking; this mechanism precedes the large rotations which cause the fiber fracture that determines the band width. [It is highly encouraging that Sutcliffe and Fleck (1994) have observed matrix cracks in microbuckle tips, ahead of the propagating kink band where the fibers are broken. They also observed extensive cracking in the kink band itself.]

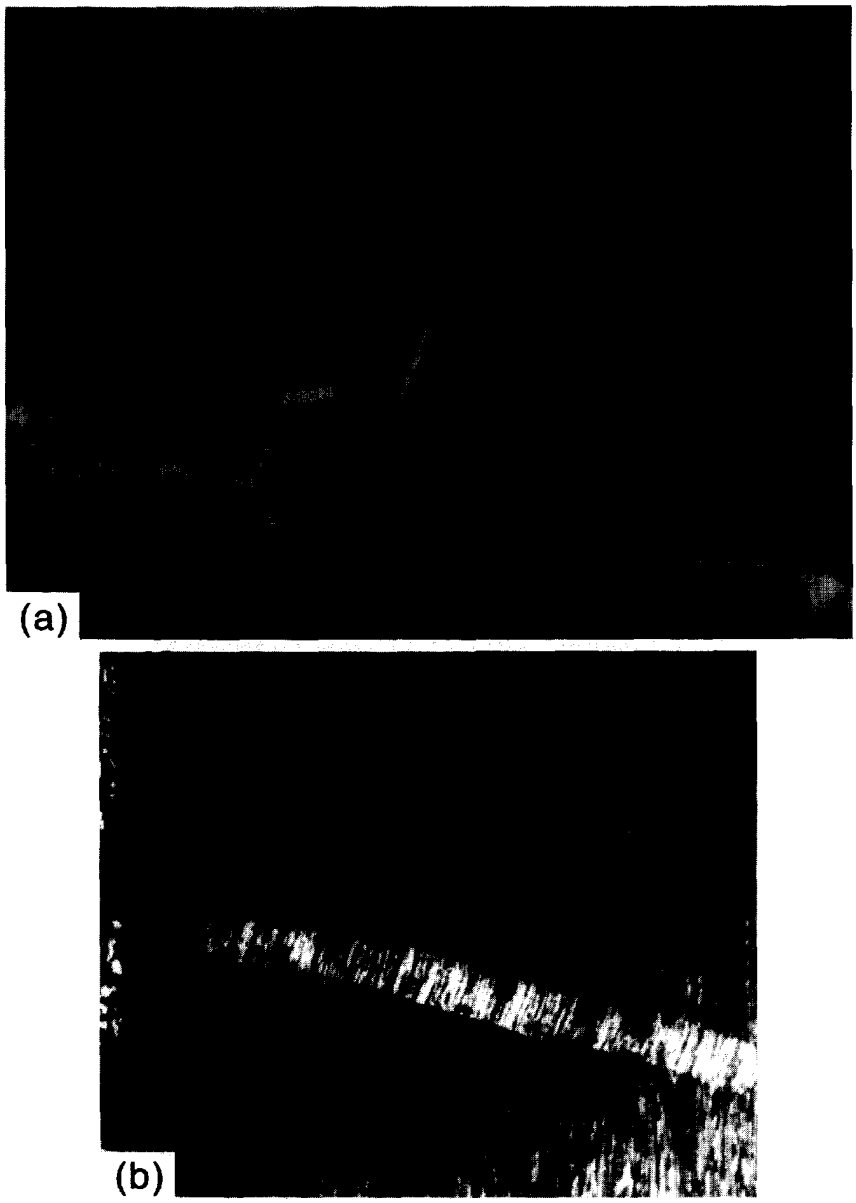

Fig. 1. Examples of kink bands: (a) kink band in a carbon/epoxy (IM6G/3501-6) composite (Daniel, 1994). The fiber diameter is 4–4.5 μm; (b) kink bands in a carbon/PEEK (AS4/APC-2) composite (Kyriakides *et al.*, 1995). The fiber diameter is 7 μm.

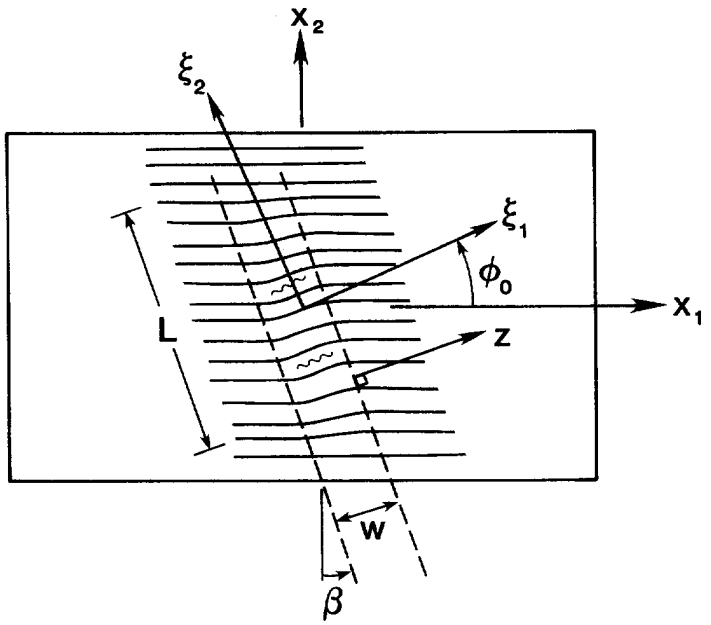

Fig. 2. Initial geometry of a unidirectional composite showing a band of misaligned fibers. The initial, local misalignment angle is ϕ_0 and the local principal material coordinates are (ξ_1, ξ_2). Possible locations for induced matrix cracking are indicated by $\sim\sim\sim$.

Referring to Fig. 2, the initial imperfection used in our analysis is assumed to be defined by an initial fiber misalignment angle $\phi_0(z)$, where the length-to-width L/W is large enough to permit the use of a local, one-dimensional analysis. How ϕ_0 varies with z in the band is arbitrary as long as its gradient is small enough to permit the use of effectively homogeneous composite properties.

We should emphasize, however, that our initial band may in fact be the result of elastic deformations, as proposed by Budiansky (1983). Alternatively, if the analysis of Kyriakides *et al.* (1995) were generalized by defining initial waviness with respect to a rotated coordinate system (so that their waviness pattern is rotated through an arbitrary angle, not necessarily β), then we may be able to interpret our deformed band as that which is expected to come from a strain localization process. In both of these cases, ϕ_0 would have to be viewed as an "effective" initial misalignment angle. In our analysis we assume a long band of misaligned fibers exists in the initial, unstressed state. If it does not, but instead develops from a strain localization process, then without further study it is not clear how accurate the predictions are. Presently, we are motivated by the simplicity of the one-dimensional analysis and encouraged by the realistic kink band widths predicted by Fleck *et al.* (1993) and earlier strength predictions, both using one-dimensional analyses.

Fortunately, the value of β predicted for kink bands is shown later to be *insensitive* to ϕ_0. However, β is found to be *sensitive* to the stress normal to the fibers in the region of strong shear nonlinearity. Constitutive idealizations used by most authors who have studied the compressive failure problem, such as elastic–perfectly plastic behavior and the Ramberg–Osgood, power law representation are not accurate enough to provide realistic values of this normal stress for the carbon/epoxy composite material studied here. Therefore, in Section 2 we develop a detailed material characterization which is then used in the subsequent study. In view of the need for an accurate normal stress prediction, the analysis in Section 3 allows for arbitrarily large geometric nonlinearities and does *not* assume the fibers are inextensible; also, general in-plane loading is treated. For comparison purposes, a geometrically approximate solution is developed in Section 4. Apart from the use here of a more general constitutive equation and a rigid body rotation, this solution is comparable

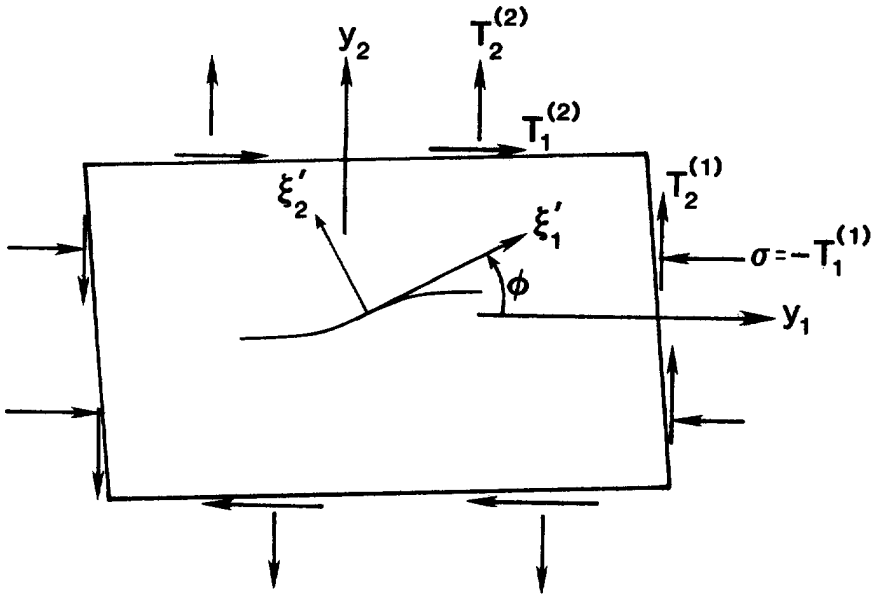

Fig. 3. Deformed geometry showing applied tractions and current, local fiber angle ϕ in band with misaligned fibers. The compressive stress in the initial average fiber direction is σ. Current global coordinates (y_1, y_2) are parallel to initial global coordinates (x_1, x_2).

to that developed by Slaughter *et al.* (1992). Section 5 gives several results based on the exact and approximate formulations, and also discusses the prediction of kink band angle. Most results are for a state of plane strain, but some predictions for plane stress are given. For in-plane kink bands, the most realistic idealization would be based on generalized plane stress. However, we have found that results for this case are graphically indistinguishable from those for plane strain; no analysis details are given for the former case.

2. CONSTITUTIVE EQUATIONS

Two-dimensional, linear elastic constitutive equations for a unidirectional fiber composite referred to the local *initial* principal material coordinates, ξ_1 and ξ_2 (cf. Fig. 2) are

$$\varepsilon_1 = S_{11}\sigma_1 + S_{12}\sigma_2 \tag{1}$$

$$\varepsilon_2 = S_{12}\sigma_1 + S_{22}\sigma_2 \tag{2}$$

$$\gamma_{12} = S_{66}\tau_{12} \tag{3}$$

in which Jones' (1975) notation is used. Figure 3 shows the notation used in defining the deformed state. For plane stress, the compliances S_{ij} in terms of familiar engineering material parameters are

$$S_{11} = 1/E_1, \quad S_{12} = -\nu_{12}/E_1, \quad S_{22} = 1/E_2, \quad S_{66} = 1/G_{12} \tag{4}$$

in which E_1 and E_2 are the Young's moduli for uniaxial stressing parallel and perpendicular to the fiber direction, respectively. Also, ν_{12} is the Poisson's ratio for loading in the fiber direction and G_{12} is the shear modulus. In the context of the present nonlinear theory, these quantities are interpreted as secant values. For plane strain, it is easily shown that eqns (1)–(3) may be used if, instead of eqn (4), we use

$$S_{11} = 1/\hat{E}_1, \quad S_{12} = -\hat{v}_{12}/\hat{E}_1, \quad S_{22} = 1/\hat{E}_2, \quad S_{66} = 1/G_{12} \tag{5}$$

where

$$\hat{E}_1 = E_1/(1-v_{12}v_{21}), \quad \hat{E}_2 = E_2/(1-v_{23}^2) \tag{6}$$

$$\hat{v}_{12} = v_{12}(1+v_{23})/(1-v_{12}v_{21}), \quad v_{21} = v_{12}E_2/E_1 \tag{7}$$

and the composite has been assumed to be transversely isotropic, i.e. isotropic in the $\xi_2-\xi_3$ plane, where ξ_3 is normal to the plane of the page. The Poisson's ratios v_{21} and v_{23} are defined as $v_{21} \equiv -\varepsilon_1/\varepsilon_2$ and $v_{23} \equiv -\varepsilon_3/\varepsilon_2$, where these strains are due to a uniaxial stress normal to the fibers.

The approach to characterizing nonlinear behavior employed by Schapery (1989) for a carbon/epoxy composite consists of using eqns (1)–(4), but with a generalization in which the material parameters in eqn (4) vary with an internal state variable (ISV) S and with fiber strain ε_1 (except for G_{12}). The dependence on ε_1 was found to be elastic (i.e. independent of strain history), which accounted for the commonly observed increase in E_1 and decrease in v_{12} with an increase in fiber tensile strain. This dependence was relatively weak and will be neglected here. Changes in only E_2 and G_{12} accounted for most of the nonlinearity exhibited by the unidirectional composite; as before, they will be characterized here through their dependence on S. This ISV is viewed as one that reflects changes in the microstructure, such as shear banding in the matrix as well as microcracking in the matrix and fiber–matrix debonding; as such, S is called a *structural parameter*. More than one ISV could be used, but one was found to be sufficient for the unidirectional composite. In the absence of a free energy of healing, the second law of thermodynamics allows only those changes for which (Schapery, 1990)

$$\mathrm{d}S/\mathrm{d}t \geqslant 0. \tag{8}$$

Studies of toughened and untoughened graphite/epoxy composite under multiaxial loading have shown that the work of deformation is not sensitive to the loading path for a wide range of paths (Lamborn and Schapery, 1993). A necessary and sufficient condition for complete path independence of work whenever $\mathrm{d}S/\mathrm{d}t > 0$ is that (Schapery, 1990),

$$\partial W/\partial S = -1. \tag{9}$$

As used here, W is the strain energy density expressed in terms of strains and S; for S fixed, W is the work of straining for unit initial volume. Also, S is the total work input W_T less the strain energy density,

$$S = W_T - W \tag{10}$$

and thus may be interpreted as the work/initial volume required to change the material's microstructure. With $[Q_{ij}] = [S_{ij}]^{-1}$, then

$$W = \tfrac{1}{2}(Q_{11}\varepsilon_1^2 + Q_{22}\varepsilon_2^2 + 2Q_{12}\varepsilon_1\varepsilon_2 + Q_{66}\gamma_{12}^2). \tag{11}$$

Alternatively, the complementary strain energy density $W_c = -W + \sigma_i\varepsilon_i$ may be used,

$$W_c = \tfrac{1}{2}(S_{11}\sigma_1^2 + S_{22}\sigma_2^2 + 2S_{12}\sigma_1\sigma_2 + S_{66}\tau_{12}^2). \tag{12}$$

In this case, it is readily shown that eqn (9) is to be replaced by

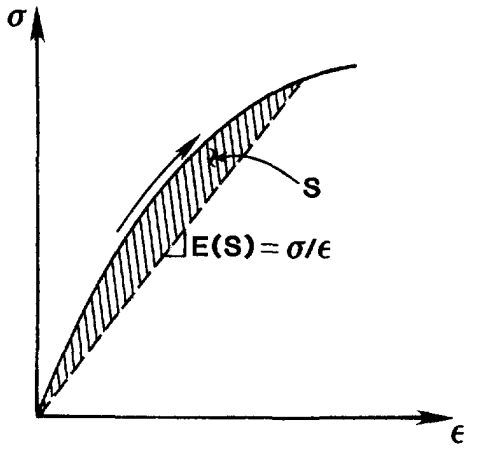

Fig. 4. Stress–strain curve for uniaxial loading in arbitrary (x) direction. The internal state variable S is equal to the shaded area. The dashed line is not necessarily the unloading stress–strain curve.

$$\partial W_c/\partial S = 1. \tag{13}$$

Figure 4 shows the significance of S for a single stress–strain pair. It should be emphasized that the straight line drawn from the origin to the current strain is not necessarily the unloading line. In contrast to metal-like plasticity theory, unloading behavior and residual strains, if any, may be uncoupled from loading behavior (Schapery, 1989). In view of eqn (10), S is equal to the shaded area.

Characterization of a carbon/epoxy composite

As described by Schapery (1989) in a study of Hercules' AS4/3502 carbon/epoxy composite, the secant moduli E_2 and G_{12} in eqn (4) were found first as functions of the axial strain ε in uniaxial stress tests, and then expressed in terms of S; for each strain level in a test, eqn (10) provides the corresponding value of S. The functions E_2 and G_{12} were observed to vary linearly in strain for very small strains. When $|\varepsilon| \ll 1$, it follows that $W_T \simeq W \sim \varepsilon^2$, and thus $S \sim \varepsilon^3$. As a result, in curve-fitting the data, one may express E_2 and G_{12} as polynomials in S_r, where

$$S_r \equiv S^{1/3}. \tag{14}$$

More generally, if the *change* in a modulus is $0(\varepsilon^N)$ as $\varepsilon \to 0$, then $S = 0(\varepsilon^{2+N})$, and the appropriate expansion parameter is $S^{N/(2+N)}$.

Figure 5 illustrates the shear stress–strain behavior as extracted from a $[\pm 45]_{3s}$ laminate, and Fig. 6 gives $S_{22} \equiv 1/E_2$ and $S_{66} \equiv 1/G_{12}$ as functions of S_r. In both figures the solid

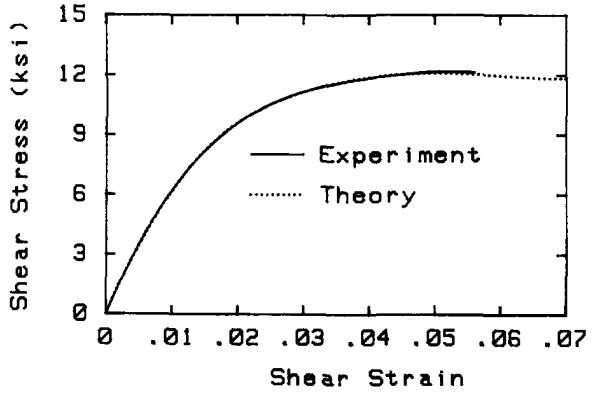

Fig. 5. Principal shear stress (τ_{12})–strain (γ_{12}) behavior. The theoretical (dotted) curve is based on the polynomial representation of the S_{66} compliance in Fig. 6 and on eqn (9), with $\varepsilon_1 = \varepsilon_2 = 0$; this equation (in terms of $G_{12} = 1/S_{66}$) was used to relate S_r to shear strain.

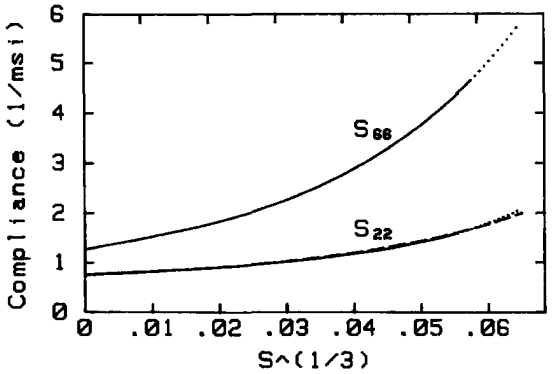

Fig. 6. Shear (S_{66}) and transverse (S_{22}) secant compliances for plane stress as functions of the internal state variable $S_r = S^{1/3}$. The dashed line is based on the use of eqn (16), $C = 3.66$ and $S_{220} = 1/1.34$ to predict S_{22}. The dotted lines are extrapolations out to the same limiting S_r value used in Fig. 5.

lines are from experimental data taken out to the point of specimen tensile failure or observable cracking. Sixth order polynomials in S_r give accurate representations of both compliances; the coefficients are given in Table 1. The dotted lines are extrapolations of the polynomial representations slightly beyond the S_r value at which the maximum shear stress in Fig. 5 occurs; the limiting value $S_r = 0.066$ in Fig. 6 provides the value $\gamma_{12} = 0.070$ in Fig. 5. The moduli E_2 and G_{12} are from $\theta = 15°$ unidirectional and $\theta = \pm 45°$ angle-ply specimens, respectively. Several other unidirectional and angle-ply composite tests were conducted and essentially the same $G_{12}(S_r)$ was found for all cases. However, $E_2(S_r)$ varied somewhat from one type of specimen to another type. A follow-up study by Sicking (1992) showed that one function $E_2(S_r)$ is obtained when the stress normal to the fibers is tensile (off-axis, unidirectional composites), and a somewhat larger $E_2(S_r)$ is obtained when this normal stress is compressive ($\pm 30°$ angle-ply composite); this behaviour is physically reasonable if microcracking or microfissuring contributes to the nonlinear behavior. The subsequent kink band analysis predicts a tensile stress normal to the fibers (except in the neighborhood of $\beta = 0°$), and therefore a characterization based on the $\theta = 15°$ unidirectional composite is used here. We should add that $\pm 45°$ laminates provided G_{12} out to the largest value of S_r(= 0.058), among all lay-ups studied. The next largest S_r(= 0.056) was found at the ultimate stress for the $\theta = 15°$ specimens. The $\pm 45°$ laminate response is insensitive to E_2 and thus to S_{22}; this compliance was therefore obtained from the $\theta = 15°$ specimens. For reference purposes, we note that in the linear elastic range of behaviour the polynomial fits provide $E_2 = 1.34$ msi and $G_{12} = 0.794$ msi; also, $E_1 = 18.2$ msi and $\nu_{12} = 0.334$. These constants and polynomial coefficients in Table 1 were used to develop the results covered in Section 5.

It has been found that variations in S_{66} and S_{22} are related very simply. Specifically, define

$$\Delta S_{66} \equiv S_{66} - S_{660}, \quad \Delta S_{22} \equiv S_{22} - S_{220} \tag{15}$$

where $S_{660} = S_{66}(0)$ and $S_{220} = S_{22}(0)$.

Table 1. Polynomial coefficients for S_{22} and S_{66}

Exponent	0	1	2	3	4	5	6
S_{22}	0.747	5.46	180	−8000	32E+4	−5.28E+6	3.76E+7
S_{66}	1.26	27.6	−260	14700	125E+3	−4.89E+6	4.36E+7

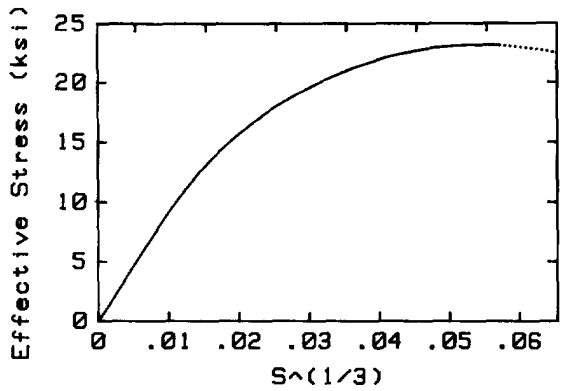

Fig. 7. Effective stress σ_0 in eqn (20) with $C = 3.66$, as a function of $S_r = S^{1/3}$.

Then

$$\Delta S_{66} = C\Delta S_{22} \tag{16}$$

where $C = 3.66$. The maximum difference between the given ΔS_{22} and that predicted from eqn (16) is less than 2% for $S_r \leqslant 0.066$; the coefficients in Table 1 do not satisfy this ratio as they were obtained directly from experimental values of S_{22} and S_{66}. It should be noted that $S_{660}/S_{220} = 1.68$, and therefore the ratio S_{66}/S_{22} is *not* constant even when eqn (16) is used.

Equations (1)–(3) and (13) are used in the subsequent analysis. The latter equation enables S to be found, given the stresses. In terms of S_r, eqn (13) may be written in the form

$$\frac{1}{S_r}\left(\frac{\partial W_c}{\partial S_r} - 3S_r^2\right) = 0. \tag{17}$$

We have used the Newton–Raphson method to find S_r by driving the left side to zero; the indicated division by S_r is found to increase the rate of convergence so that, typically, only one or two iterations are required for each given stress state, as the stresses are changed stepwise. When S_r is very small convergence is not usually achieved; but for small values of S_r iteration is not needed. Specifically, from eqns (12) and (17) we have

$$S_r = \left[\frac{1}{6}\left(\frac{dS_{11}}{dS_r}\sigma_1^2 + \frac{dS_{22}}{dS_r}\sigma_2^2 + 2\frac{dS_{12}}{dS_r}\sigma_1\sigma_2 + \frac{dS_{66}}{dS_r}\tau_{12}^2\right)\right]^{1/2}. \tag{18}$$

Thus, if $S_r \ll 1$ the derivatives may be evaluated at $S_r = 0$, and eqn (18) then provides S_r explicitly; it is also useful in providing a first guess for S_r in an iteration process when S_r is small. The combination of eqns (17) and (18) always leads quickly to converged values of S_r for all cases studied.

Characterization in terms of an effective stress

Next, let us consider certain implications of eqn (16), which is based on the plane stress version of S_{22} in eqn (4). Given that E_1 and ν_{12} are constants, and using eqn (12) for plane stress, we find eqn (17) may be written in the form

$$\frac{dS_{22}}{dS_r}\sigma_0^2 = 6S_r^2 \tag{19}$$

where

$$\sigma_0^2 \equiv \sigma_2^2 + C\tau_{12}^2. \tag{20}$$

Equation (19) implies that S_r depends on the stress state through one *effective stress* σ_0. This relationship is drawn in Fig. 7. The maximum in σ_0 occurs at $S_r \simeq 0.054$, which is the

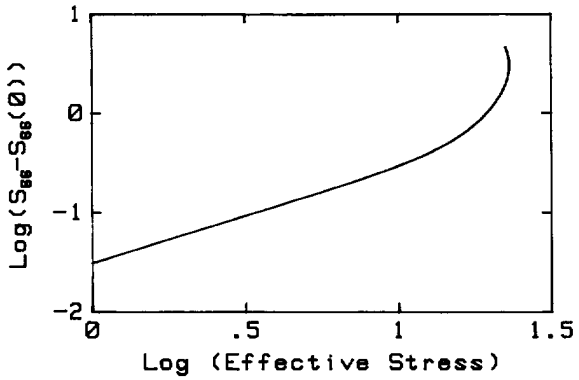

Fig. 8. Change in shear compliance (msi^{-1}) as a function of σ_0 (ksi) on logarithmic (base 10) coordinates.

same value of S_r as that for which the maximum shear stress in Fig. 5 is reached. That the nonlinear behavior is fully characterized in terms of σ_0 (for $S_r < 0.054$) is in agreement with the work of Lou and Schapery (1971) ($C = 3.88$) and Mignery and Schapery (1991) ($C = 4$) on nonlinear viscoelastic behavior of glass/epoxy and carbon/rubber-toughened epoxy composites, respectively, and with that for time independent behavior reported by Sun and Chen (1989) on carbon/epoxy ($C = 2.5$) and boron/aluminum ($C = 4$) and by Sun and Rui (1990) on carbon/PEEK ($C = 3.4$).

For plane strain, eqns (5)–(7) are needed to evaluate the derivatives of S_{ij}. The Poisson's ratio ν_{23} is required for this case. The author is not aware of any published studies on ν_{23} which deal with its possible dependence on S_r, σ_0 or any other parameter. Here, we shall assume ν_{23} is constant in order to illustrate the difference between plane stress and plane strain results. Then, from eqn (17) and recalling that E_1, ν_{12} and ν_{23} are assumed constant, we find

$$\frac{dS_{22}}{dS_r}\hat{\sigma}_0^2 = 6S_r^2 \tag{21}$$

where $S_{22} = 1/E_2$ is the compliance for plane *stress* and

$$\hat{\sigma}_0^2 = \nu_{21}^2\sigma_1^2 + (1-\nu_{23}^2)\sigma_2^2 + C\tau_{12}^2. \tag{22}$$

It is seen that σ_1 now enters the equation for S_r. Additionally, ν_{21} is proportional to E_2 and thus the quantity $\hat{\sigma}_0$ is a function of S_r besides σ_1. Nevertheless, the relationship between $\hat{\sigma}_0$ and S_r is the same as that in Fig. 7 if σ_0 is replaced by $\hat{\sigma}_0$ [cf. eqns (19) and (21)].

For the stress state in a deformed band we have found that the term $\nu_{21}^2\sigma_1^2$ is negligible because $\nu_{21} \ll 1$ [unless ϕ_0 is unrealistically low ($\phi_0 < 0.1°$) or β is exceptionally high ($\beta > 30°$) as they result in large values of σ_1]. Thus, as in the plane stress case, there is a one-to-one correspondence between S_r and an effective stress (up to the maximum point in Fig. 7) which is a quadratic function of the ply stresses. We may therefore express the compliances directly in terms of the effective stress instead of S_r for $S_r < 0.054$. Figure 8 shows how ΔS_{66} varies with σ_0 on logarithmic (base 10) coordinates.

Clearly, ΔS_{66} does *not* obey a power law in σ_0 except at low stresses (where the exponent is unity), in contrast to the approximate power law behavior reported for some other composites [e.g. Sun and Chen (1989) and Mignery and Schapery (1991)]. Moreover, a polynomial or power law representation is *not* sufficient to characterize behavior out to the vertical tangent; this limiting behavior is needed in the prediction of the kink band angle, as shown later. Therefore, even if eqn (16) is employed, it is best to not use effective stress but, instead, to retain the use of S_r and eqns (19) and (21) in the analysis.

3. ANALYSIS OF A MISALIGNED FIBER BAND

Kinematics

As discussed in the Introduction and illustrated in Fig. 2, the initial imperfection is assumed to be fiber waviness which is defined by a fiber misalignment angle ϕ_0 that varies in only one direction; namely, $\phi_0 = \phi_0(z)$, where

$$z = x_1 + \ell x_2 \tag{23}$$

and

$$\ell = \tan\beta. \tag{24}$$

Also, x_1 and x_2 are the initial *global* coordinates. The in-plane displacements $(\hat{u}_1, \hat{u}_2)$ are taken in the form

$$\hat{u}_1 = a_{11}x_1 + a_{12}x_2 + u_1 \tag{25}$$

$$\hat{u}_2 = a_{21}x_1 + a_{22}x_2 + u_2 \tag{26}$$

where the a_{ij} are constants, and $u_i = u_i(z)$ are the displacements due to fiber waviness. For perfectly straight fibers $u_1 = u_2 = 0$, and the resulting displacements define a uniform strain field plus a rigid rotation (as given by a_{ij}). If $a_{21} = 0$ then there is no rigid fiber rotation; however, a general array a_{ij} is used here as all components may be needed for each layer in a structural analysis of a multi-directional fiber laminate.

The displacement derivatives are

$$\partial\hat{u}_1/\partial x_1 = a_{11} + u_1', \quad \partial\hat{u}_1/\partial x_2 = a_{12} + \ell u_1' \tag{27}$$

$$\partial\hat{u}_2/\partial x_1 = a_{21} + u_2', \quad \partial\hat{u}_2/\partial x_2 = a_{22} + \ell u_2' \tag{28}$$

where here, and in what follows, the prime denotes a derivative with respect to z. We shall use Green's strains E_{ij} (Fung, 1965) in the constitutive equations in order to allow for geometric nonlinearities. It follows that

$$E_{11} = a_{11} + u_1' + \tfrac{1}{2}[(a_{11} + u_1')^2 + (a_{21} + u_2')^2] \tag{29}$$

$$E_{22} = a_{22} + \ell u_2' + \tfrac{1}{2}[(a_{12} + \ell u_1')^2 + (a_{22} + \ell u_2')^2] \tag{30}$$

$$2E_{12} = a_{12} + a_{21} + \ell u_1' + u_2' + [(a_{11} + u_1')(a_{12} + \ell u_1') + (a_{21} + u_2')(a_{22} + \ell u_2')]. \tag{31}$$

Also needed is the local fiber angle ϕ expressed in terms of the initial fiber angle ϕ_0 and the displacements. With y_i defining the instantaneous geometry, so that $y_i = x_i + \hat{u}_i$, then from Fig. 9,

$$\tan\phi = \frac{\mathrm{d}y_2}{\mathrm{d}y_1} = \frac{\partial\hat{u}_2/\partial x_1 + (1 + \partial\hat{u}_2/\partial x_2)\tan\phi_0}{1 + \partial\hat{u}_1/\partial x_1 + (\partial\hat{u}_1/\partial x_2)\tan\phi_0} \tag{32}$$

and using eqns (27) and (28),

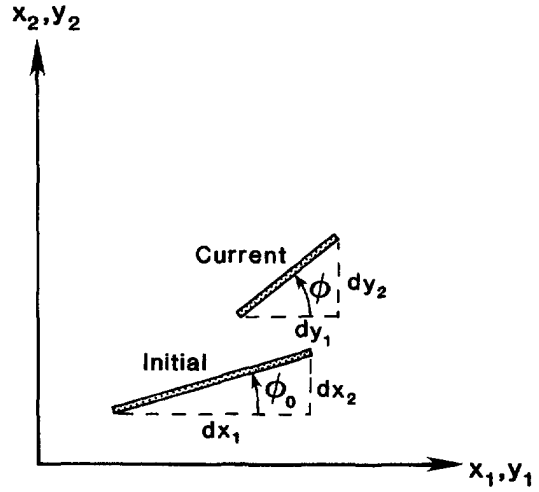

Fig. 9. Notation for predicting rotation of a material element which is initially in the fiber direction.

$$\tan\phi = \frac{a_{21} + u_2' + (1 + a_{22} + \ell u_2')\tan\phi_0}{1 + a_{11} + u_1' + (a_{12} + \ell u_1')\tan\phi_0}. \tag{33}$$

Stress tensors and the equilibrium equations

The stresses in the constitutive equations must be selected such that they are work conjugates of the strains. As Green's strain tensor is used, the symmetric *Kirchhoff*'s stress tensor (also called the second Piola–Kirchhoff stress tensor), say σ_{ij}, is the appropriate tensor (Fung, 1965). On the other hand, the equilibrium equations for arbitrarily large geometric nonlinearities are expressed most simply in terms of the nonsymmetric *Lagrangian* stress tensor (also called the first Piola–Kirchhoff stress tensor), say L_{ij} (Fung, 1965). These equations have the same form as for geometrically linear problems; namely,

$$\partial L_{11}/\partial x_1 + \partial L_{21}/\partial x_2 = 0 \tag{34}$$

$$\partial L_{12}/\partial x_1 + \partial L_{22}/\partial x_2 = 0. \tag{35}$$

The connection between the stress tensors is

$$L_{ij} = \sigma_{ik}\frac{\partial y_j}{\partial x_k} \tag{36}$$

where $y_i = x_i + \hat{u}_i$ and a repeated index implies symmation over its range. Explicitly, for the two-dimensional problem at hand,

$$L_{11} = (1 + a_{11} + u_1')\sigma_{11} + (a_{12} + \ell u_1')\sigma_{12} \tag{37}$$

$$L_{22} = (a_{21} + u_2')\sigma_{12} + (1 + a_{22} + \ell u_2')\sigma_{22} \tag{38}$$

$$L_{12} = (a_{21} + u_2')\sigma_{11} + (1 + a_{22} + \ell u_2')\sigma_{12} \tag{39}$$

$$L_{21} = (1 + a_{11} + u_1')\sigma_{12} + (a_{12} + \ell u_1')\sigma_{22}. \tag{40}$$

The symmetric *true* stress tensor, say T_{ij} (also called the Eulerian or Cauchy stress tensor) will be used later in strength predictions. It can be found from the Lagrangian stresses using

$$T_{ij} = \frac{\rho}{\rho_0} L_{kj} \frac{\partial y_i}{\partial x_k} \tag{41}$$

where ρ/ρ_0 is the ratio of current-to-initial density; this ratio is close to unity for applications of interest here, and consequently we shall omit this factor. Hence,

$$T_{11} = (1+a_{11}+u_1')L_{11} + (a_{12}+\ell u_1')L_{21} \tag{42}$$

$$T_{22} = (a_{21}+u_2')L_{12} + (1+a_{22}+\ell u_2')L_{22} \tag{43}$$

$$T_{12} = T_{21} = (1+a_{11}+u_1')L_{12} + (a_{12}+\ell u_1')L_{22}. \tag{44}$$

Constitutive equations referred to global coordinates

The constitutive equations (1)–(3) are referred to the initial principal material directions. These directions vary spacially due to initial fiber waviness, and are oriented locally at an angle ϕ_0 relative to the global coordinate directions. The strains ε_1, ε_2 and $\gamma_{12}/2$ are components of Green's strain tensor referred to the coordinates (ξ_1, ξ_2). Similarly, σ_1, σ_2 and τ_{12} are components of Kirchhoff's stress tensor referred to (ξ_1, ξ_2). The kink band problem is conveniently solved using constitutive equations referred to the global initial coordinates (x_1, x_2) in which stresses σ_{ij} are expressed as functions of strains E_{ij}. Starting with eqns (1)–(3), the resulting equations are identical in form to those for linear elastic behavior, and thus may be taken directly from Jones (1975, p. 51),

$$\sigma_{11} = \bar{Q}_{11}E_{11} + \bar{Q}_{12}E_{22} + 2\bar{Q}_{16}E_{12} \tag{45}$$

$$\sigma_{22} = \bar{Q}_{12}E_{11} + \bar{Q}_{22}E_{22} + 2\bar{Q}_{26}E_{12} \tag{46}$$

$$\sigma_{12} = \bar{Q}_{16}E_{11} + \bar{Q}_{26}E_{22} + 2\bar{Q}_{66}E_{12} \tag{47}$$

where

$$\bar{Q}_{11} = Q_{11}c_p^4 + 2(Q_{12}+2Q_{66})s_p^2c_p^2 + Q_{22}s_p^4 \tag{48a}$$

$$\bar{Q}_{12} = (Q_{11}+Q_{22}-4Q_{66})s_p^2c_p^2 + Q_{12}(s_p^4+c_p^4) \tag{48b}$$

$$\bar{Q}_{22} = Q_{11}s_p^4 + 2(Q_{12}+2Q_{66})s_p^2c_p^2 + Q_{22}c_p^4 \tag{48c}$$

$$\bar{Q}_{16} = (Q_{11}-Q_{12}-2Q_{66})s_pc_p^3 + (Q_{12}-Q_{22}+2Q_{66})s_p^3c_p \tag{48d}$$

$$\bar{Q}_{26} = (Q_{11}-Q_{12}-2Q_{66})s_p^3c_p + (Q_{12}-Q_{22}+2Q_{66})s_pc_p^3 \tag{48e}$$

$$\bar{Q}_{66} = (Q_{11}+Q_{22}-2Q_{12}-2Q_{66})s_p^2c_p^2 + Q_{66}(s_p^4+c_p^4) \tag{48f}$$

in which

$$c_p \equiv \cos\phi_0, \quad s_p \equiv \sin\phi_0 \tag{49}$$

and $Q_{ij} = [S_{ij}]^{-1}$. For plane stress [cf. eqn (4)],

$$Q_{11} = E_1/D, \quad Q_{22} = E_2/D, \quad Q_{12} = \nu_{12}E_2/D$$
$$Q_{66} = G_{12}, \quad D = 1-\nu_{12}^2E_2/E_1. \tag{50}$$

For plane strain, replace (E_1, E_2, ν_{12}) by $(\hat{E}_1, \hat{E}_2, \hat{\nu}_{12})$ using eqns (6) and (7).

The $\bar{Q}_{ij}$ depend on the internal state variable S. This ISV may be derived from eqn (9), in which W is expressed in terms of Q_{ij} or $\bar{Q}_{ij}$ and the appropriate strains. However, we may take advantage of the simplification in eqn (16) by using eqn (19) for plane stress or eqn

(21) for plane strain. The stresses in these two equations are referred to the (ξ_1, ξ_2) coordinates, which may be found from σ_{ij} using the tensor transformation,

$$\sigma_1 = \sigma_{11}c_p^2 + \sigma_{22}s_p^2 + 2\sigma_{12}s_pc_p \tag{51}$$

$$\sigma_2 = \sigma_{11}s_p^2 + \sigma_{22}c_p^2 - 2\sigma_{12}s_pc_p \tag{52}$$

$$\tau_{12} = (\sigma_{22} - \sigma_{11})s_pc_p + \sigma_{12}(c_p^2 - s_p^2). \tag{53}$$

Boundary conditions

Tractions or displacements will be specified on the boundaries where $\phi_0 = 0$, i.e. outside of the misaligned fiber band. This one-dimensional analysis does not provide the freedom to specify conditions on surfaces $x_2 =$ constant where $\phi_0 \neq 0$. It is assumed that the band is narrow enough so that the error in not meeting the boundary conditions is limited to a relatively small zone near its ends.

Surface tractions T_i (force/initial area) are simply related to the initial unit normal n_i and Lagrangian stresses L_{ij} through

$$T_i = L_{ji}n_j. \tag{54}$$

Thus, on the surface for which $n_1 = 1$,

$$T_1^{(1)} = L_{11}^{\circ}, \quad T_2^{(1)} = L_{12}^{\circ} \tag{55a}$$

and on $n_2 = 1$,

$$T_1^{(2)} = L_{21}^{\circ}, \quad T_2^{(2)} = L_{22}^{\circ} \tag{55b}$$

where the superscript "$\circ$" indicates that the stresses are evaluated in the uniformly stressed region outside of the band, i.e. where $\phi_0 = u_1' = u_2' = 0$. Of course, one may specify either the boundary displacements by giving the four constants a_{ij}, or the tractions $T_i^{(j)}$, or displacement–traction combinations such as a_{11} and $T_2^{(1)}$.

General solution

The Lagrangian stresses in the band may be expressed in terms of u_1' and u_2' by substituting eqns (29)–(31) into (45)–(47) and then using eqns (37)–(40). Spacewise variation of these stresses is entirely through z [eqn (23)]. Equilibrium eqns (34) and (35) become

$$L_{11}' + \ell L_{21}' = 0, \quad L_{12}' + \ell L_{22}' = 0. \tag{56}$$

Upon integration with respect to z and expressing the constants of integration in terms of stresses outside of the band, we find

$$L_{11} + \ell L_{21} = L_{11}^{\circ} + \ell L_{21}^{\circ} \tag{57}$$

$$L_{12} + \ell L_{22} = L_{12}^{\circ} + \ell L_{22}^{\circ}. \tag{58}$$

The two unknowns, u_1' and u_2', may be found from these two equations. Observe that they are simply nonlinear algebraic equations in terms of local values of the unknowns and the local, given value of ϕ_0. They may be readily solved by standard numerical methods, such as the Newton–Raphson method. The axial compressive load exhibits a maximum with respect to the shear variable u_2', and thus to avoid a numerical instability problem we used u_2' as an independent variable and the axial traction $T_1^{(1)}$ or strain a_{11} as a dependent variable.

4. APPROXIMATE SOLUTION

A simple solution for kink band response can be found by a perturbation analysis in which terms of only the lowest comparable order in small parameters are retained in each equation. Here, the relevant parameters are initial misalignment angle ϕ_0, a measure of strain magnitude at failure, designated by ε, and initial modulus ratio,

$$\alpha = G_{12}(0)/E_1. \tag{59}$$

These three parameters are assumed to be of the same order of magnitude. Similarly, we assume E_2, G_{12} and σ_{11} are of the same order of magnitude; that σ_{11} and G_{12} are comparable comes from a preliminary analysis (or existing microbuckling or kink band solutions). Inasmuch as $\alpha \ll 1$ and $\nu_{12} \simeq 1/3$ (typically), in eqn (50) we may set $D = 1$ and consider Q_{22}, Q_{12} and Q_{66} to be of the same order of magnitude. These assumptions are consistent with actual values of the relevant parameters for plastics reinforced with common high modulus fibers; for example, α, ϕ_0 and ε (shear strain, say) are in the neighborhood of 0.03 at axial stresses which are close to realistic compressive strengths for carbon/epoxy composites.

In a formal perturbation analysis one would first non-dimensionalize all stresses and moduli by dividing them by a constant modulus, say E_1; equivalently, in order to avoid use of new symbols, one may take $E_1 = 1$ in the analysis and then return E_1 to its actual value in the final results. All response variables would be expanded in powers of the small parameters and the governing equations for the coefficients developed by equating terms of comparable order in each equation. Here, for simplicity, we shall develop just the lowest order solution, which turns out to be first order for strain-like quantities and axial normal stress, and second order for the other stresses; alternatively, one may first divide these latter stresses by α so that the lowest order solution for all variables is first order. One can verify that the complete lowest order solution may be found by retaining only terms of the lowest comparable order in each equation, without explicitly introducing series expansions and normalized stresses.

With this latter observation in mind, we retain only the linear terms in eqns (29)–(31) for E_{ij} and find that eqn (48) reduces to

$$\begin{aligned} &\bar{Q}_{11} = Q_{11}, \quad \bar{Q}_{12} = Q_{12}, \quad \bar{Q}_{22} = Q_{22} \\ &\bar{Q}_{16} = Q_{11}\phi_0, \quad \bar{Q}_{26} = 0, \quad \bar{Q}_{66} = Q_{66}. \end{aligned} \tag{60}$$

The stresses in eqns (45)–(47) become

$$\sigma_{11} = Q_{11}(a_{11} + u_1') \tag{61a}$$

$$\sigma_{22} = Q_{12}(a_{11} + u_1') + Q_{22}(a_{22} + \ell u_2') \tag{61b}$$

$$\sigma_{12} = Q_{11}\phi_0(a_{11} + u_1') + Q_{66}(a_{12} + a_{21} + \ell u_1' + u_2'). \tag{61c}$$

Observe that σ_{11} is a first order quantity while σ_{22} and σ_{12} are second order quantities (i.e. proportional to $\alpha\epsilon$ or $\phi_0\epsilon$). Also, from eqns (37)–(40),

$$L_{11} = \sigma_{11}, \quad L_{22} = \sigma_{22}, \quad L_{12} = (a_{21} + u_2')\sigma_{11} + \sigma_{12}, \quad L_{21} = \sigma_{12}. \tag{62}$$

Consider now the equilibrium equation (57). From eqns (61) and (62), L_{11} is a first order quantity while L_{21} is second order. Thus,

$$L_{11} = L_{11}^{\circ}, \quad \sigma_{11} = \sigma_{11}^{\circ} \tag{63}$$

which, together with eqn (61a), implies $u_1' = 0$ (i.e. it is at least a second order variable, which is one order higher than the other displacement derivatives). As noted previously $D = 1$ [cf. eqn (50)] since $\alpha \ll 1$; therefore $Q_{11} = E_1 = Q_{11}^{\circ}$, recalling that E_1 is constant.

As before, the superscript "○" indicates a quantity that is evaluated in the region outside of the band. With these results and eqns (61) and (62), we find eqn (58) becomes

$$Q_{11}a_{11}(\phi_0+u_2')+(Q_{66}+\ell^2Q_{22})u_2' = (Q_{66}^\circ-Q_{66})(a_{12}+a_{21}) + \ell[(Q_{12}^\circ-Q_{12})a_{11}+(Q_{22}^\circ-Q_{22})a_{22}]. \quad (64)$$

In order to predict S_r let us refer the stresses to the initial principal material coordinates (ξ_1, ξ_2). Equations (51)–(53) yield, approximately,

$$\sigma_1 = \sigma_{11}, \quad \sigma_2 = \sigma_{22}, \quad \tau_{12} = -\sigma_{11}\phi_0+\sigma_{12}. \quad (65)$$

Then, from eqn (61) and $u_1' = 0$,

$$\sigma_1 = Q_{11}a_{11} \quad (66a)$$

$$\sigma_2 = Q_{12}a_{11}+Q_{22}(a_{22}+\ell u_2') \quad (66b)$$

$$\tau_{12} = Q_{66}(a_{12}+a_{21}+u_2'). \quad (66c)$$

The tractions in eqn (55), acting on the uniformly stressed region outside the band, are

$$T_1^{(1)} = Q_{11}a_{11}, \quad T_2^{(1)} = Q_{11}a_{11}a_{21}+Q_{66}^\circ(a_{12}+a_{21}) \quad (67a)$$

$$T_2^{(2)} = Q_{12}^\circ a_{11}+Q_{22}^\circ a_{22}, \quad T_1^{(2)} = Q_{66}^\circ(a_{12}+a_{21}). \quad (67b)$$

It is helpful to recognize from eqns (55) and (62) that the Kirchhoff stresses outside the band are

$$\sigma_1^\circ = \sigma_{11}^\circ = T_1^{(1)}, \quad \sigma_2^\circ = \sigma_{22}^\circ = T_2^{(2)}, \quad \tau_{12}^\circ = \sigma_{12}^\circ = T_1^{(2)}. \quad (68)$$

Observe also that

$$T_2^{(1)} = a_{21}T_1^{(1)}+T_1^{(2)} \quad (69)$$

and thus τ_{12}° is not equal to $T_2^{(1)}$ unless $a_{21} = 0$. If the four a_{ij} are specified, then eqn (64) enables u_2' to be found, while eqn (67) provides the surface tractions outside of the band. Equations (13) and (66), applied outside the band and locally in the band provides S_r° and S_r, respectively, for each set of a_{ij}. If, instead, one or more tractions are given, then one or more a_{ij} are determined from eqn (67).

For *plane stress* we may use eqn (50) with $D = 1$, along with the previously introduced assumptions that E_1 and ν_{12} are constant. Equations (64) and (67) become

$$E_1a_{11}(\phi_0+u_2')+(G_{12}+\ell^2E_2)u_2' = (G_{12}^\circ-G_{12})(a_{12}+a_{21})+\ell(E_2^\circ-E_2)(\nu_{12}a_{11}+a_{22}) \quad (70)$$

and

$$T_1^{(1)} = E_1a_{11}, \quad T_2^{(1)} = E_1a_{11}a_{21}+G_{12}^\circ(a_{12}+a_{21}) \quad (71a)$$

$$T_2^{(2)} = E_2^\circ(\nu_{12}a_{11}+a_{22}), \quad T_1^{(2)} = G_{12}^\circ(a_{12}+a_{21}). \quad (71b)$$

The equations for *plane strain*, in which ν_{23} is assumed constant, are obtained from eqns (70) and (71) by replacing E_2 and E_2° by $\hat{E}_2$ and $\hat{E}_2^\circ$, respectively, and ν_{12} by $\hat{\nu}_{12}$, using the definitions in eqns (6) and (7). [If ν_{23} is not constant then $\hat{\nu}_{12}$ is not constant, but eqns (64)–(69) are still applicable.] With the present formulation and the simplification in eqn (16), it

is convenient to use eqn (19) for plane stress and eqn (21) for plane strain to predict S_r° and S_r. Outside of the band S_r° is found from one of these equations by using the stresses from eqn (68), as well as eqn (67) if the a_{ij} are given. However, as mentioned previously, in order to avoid difficulties with a numerical instability, u_2' should be specified [while predicting a_{11} from eqn (64)]. Equation (66) then gives the Kirchhoff stresses, although it should be noted that Q_{12}, Q_{22} and Q_{66} are functions of S_r, and that a_{11} in eqn (64) depends on both S_r and S_r°. The fact that σ_1 does not appear in eqn (19) and it has a negligible effect in eqn (21) implies that S_r° outside of the band (for which $\phi_0 = u_1' = u_2' = 0$) does not depend on a_{11}, and thus may be found independently of the band solution, unless the other a_{ij} or tractions are coupled to a_{11} or $T_1^{(1)}$ (as, for example, in the case of proportional loading). In any event we have found that the Newton–Raphson method leads quickly to a solution for S_r and S_r°.

Consider next the special case in which all four tractions are specified and, for now, *plane stress*. Upon introducing eqn (71) into (70), and defining

$$\sigma \equiv -\sigma_1^\circ = -T_1^{(1)} \tag{72}$$

where σ is the applied axial compressive stress ($\sigma > 0$), we rewrite eqn (70) and solve for σ,

$$\sigma = \left[(G_{12}+\ell^2 E_2)u_2' - \left(1-\frac{G_{12}}{G_{12}^\circ}\right)\tau_{12}^\circ - \left(1-\frac{E_2}{E_2^\circ}\right)\ell\sigma_2^\circ\right]/(\phi_0+u_2') \tag{73}$$

where eqn (68) has been used. If there is proportional loading, where

$$R_2 \equiv \sigma_2^\circ/\sigma_1^\circ, \quad R_{12} \equiv \tau_{12}^\circ/\sigma_1^\circ \tag{74}$$

are constants, then eqn (73) becomes,

$$\sigma = (G_{12}+\ell^2 E_2)u_2'/\left[\phi_0+u_2' - \left(1-\frac{G_{12}}{G_{12}^\circ}\right)R_{12} - \left(1-\frac{E_2}{E_2^\circ}\right)\ell R_2\right]. \tag{75}$$

Observe that eqns (73) and (75) do not depend on S_r° if $\tau_{12}^\circ = \sigma_2^\circ = 0$. Whether or not there is proportional loading, we may use eqn (66) outside of the band to find,

$$a_{11} = -\sigma/E_1, \quad a_{22} = \nu_{12}\sigma/E_1 + \sigma_2^\circ/E_2^\circ, \quad a_{12}+a_{21} = \tau_{12}^\circ/G_{12}^\circ. \tag{76}$$

In turn, substitute this result into eqn (61) for stresses in the band referred to the global coordinates,

$$\sigma_{11} = -\sigma, \quad \sigma_{22} = (\sigma_2^\circ/E_2^\circ + \ell u_2')E_2 \tag{77a}$$

$$\sigma_{12} = -\sigma\phi_0 + (\tau_{12}^\circ/G_{12}^\circ + u_2')G_{12}. \tag{77b}$$

Alternatively, eqn (66) gives the stresses referred to the initial principal material coordinates,

$$\sigma_1 = -\sigma, \quad \sigma_2 = \sigma_{22}, \quad \tau_{12} = \sigma_{12} + \sigma\phi_0. \tag{78}$$

Later, we shall be concerned with predicting failure of material in the band. True stresses referred to the *current* principal material directions will be used. True stresses T_{ij} referred to the global coordinate system are in eqns (42)–(44) which, for the level of approximation used here, become simply

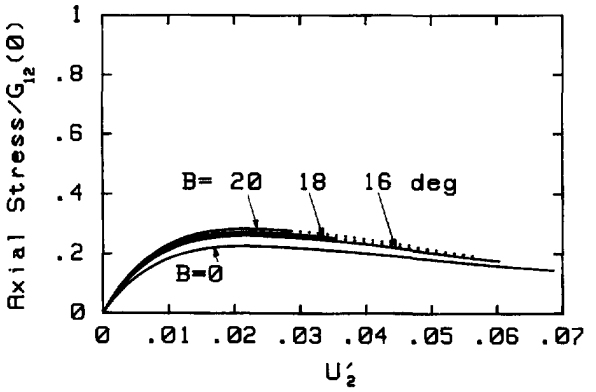

Fig. 10. Normalized axial stress as a function of du_2/dz for a range of band angles β.

$$T_{11} = L_{11}, \quad T_{22} = L_{22}, \quad T_{12} = L_{12}. \tag{79}$$

Equations (62) and (77) yield

$$T_{11} = -\sigma, \quad T_{22} = (\sigma_2^\circ/E_2^\circ + \ell u_2')E_2 \tag{80a}$$

$$T_{12} = -\sigma\phi + (\tau_{12}^\circ/G_{12}^\circ + u_2')G_{12} \tag{80b}$$

in which we have used

$$\phi = \phi_0 + a_{21} + u_2' \tag{81}$$

in view of the linearized version of eqn (33). A second order tensor transformation may be used to find true stresses referred to the current principal material axes; the transformation is the same as in eqns (51)–(53) but with $s_p = \sin\phi \simeq \phi$ and $c_p = \cos\phi \simeq 1$. Denote the true stresses in this principal material system by T_{ij}^p. Then, approximately,

$$T_{11}^p = -\sigma \tag{82a}$$

$$T_{22}^p = -\sigma\phi^2 + (\sigma_2^\circ/E_2^\circ + \ell u_2')E_2 \tag{82b}$$

$$T_{12}^p = T_{22}\phi + (\tau_{12}^\circ/G_{12}^\circ + u_2')G_{12} \tag{82c}$$

where T_{22} is in eqn (80a). Strictly speaking, the first terms $-\sigma\phi^2$ and $T_{22}\phi$ in eqns (82b) and (82c), respectively, should be omitted since they are of a higher order than the second terms. However, as described in the next section, there is a small but noticeable error in the transverse and shear stresses when these third order terms are not used. Without these latter quantities, the Kirchhoff stresses in eqn (78) and true stresses in eqn (82) are identical.

Finally, it is seen that the notation for moduli used in eqns (73)–(82) is that for plane stress. As before, the use of (^) on the moduli converts the equations to plane strain.

5. RESULTS

Various results are shown and discussed in this section. Unless stated otherwise, they are for a plane strain state, uniaxial applied stress, a representative initial misalignment angle of $\phi_0 = 2°$, and the AS4/3502 carbon/epoxy composite characterized in Section 2. In all cases $a_{12} = a_{21} = 0$.

Selected results

Figures 10 and 11 show the relationship between normalized axial compressive stress, $\sigma/G_{12}(0)$, and u_2' and E_{11}, respectively, for four different band angles. It should be mentioned that u_2' in these and succeeding figures is approximately the engineering shear strain γ_{12}.

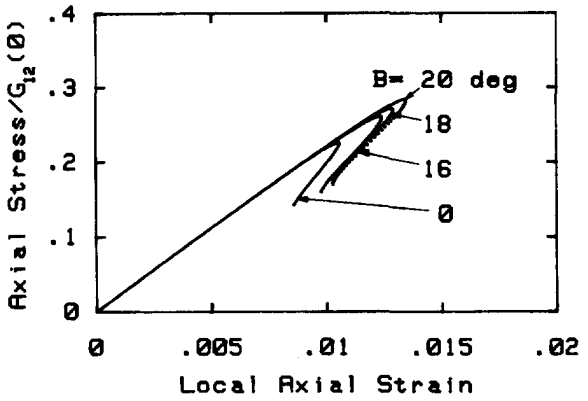

Fig. 11. Normalized axial stress as a function of the local axial strain E_{11}.

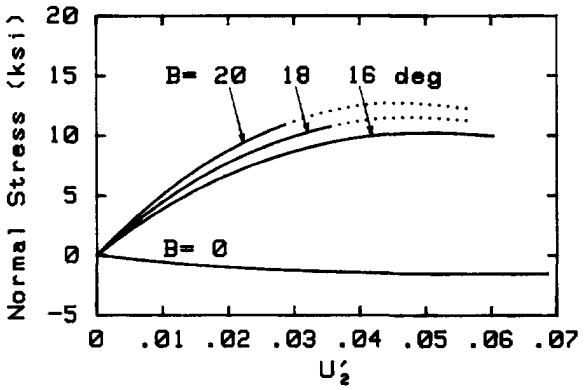

Fig. 12. True stress T^{σ}_{22} normal to the current fiber direction.

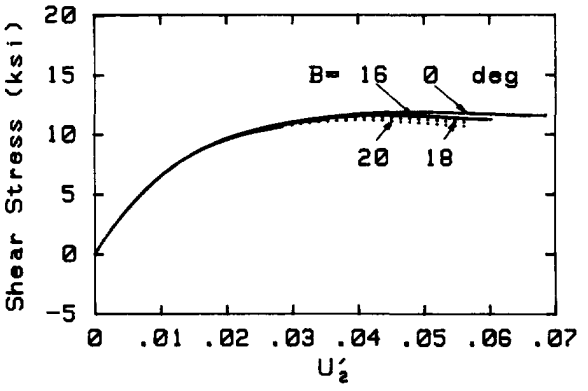

Fig. 13. True shear stress T^{σ}_{12} in the current fiber direction.

This simple relationship may be deduced by neglecting the second order terms in eqn (31), so that $2E_{12} \simeq u'_2$, and then neglecting second order terms in the strain version of eqn (53), which gives $\gamma_{12} \simeq 2E_{12}$. Figures 12 and 13 give the true normal and shear stresses, eqns (82b) and (82c), respectively, as functions u'_2. Each of the curves in Fig. 10 exhibits a maximum, which is interpreted as the compressive strength (normalized by the initial shear modulus) for a *given* band angle β. Figure 14 shows how these maxima vary with the initial misalignment angle ϕ_0 for $\beta = 0°$ and $\beta = 20°$. The normalized compressive strength for a linear elastic composite is equal to unity, and thus it is well above that predicted from the nonlinear theory unless $\phi_0 \ll 1°$. It may also be seen from this figure that the initial fiber misalignment must be extremely small to achieve a significant increase in strength over current composites (for which $\phi_0 \simeq 2°$)

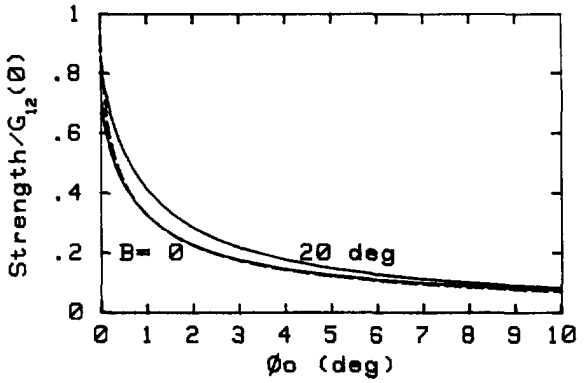

Fig. 14. Normalized compressive strength as a function of the initial fiber misalignment angle.

With the exception of the dashed line in Fig. 14, all results in Figs 10–14 are from the exact equations in Section 3. The former result is from the approximate solution, eqn (73), for $\beta = 0°$ (i.e. $\ell = 0$); in this case there is no difference between results for plane stress and plane strain. No other approximate solutions are drawn in these figures as they are very close to the exact results. Typically, the difference is no more than 5% (one or two line thicknesses) such as is illustrated in Fig. 14. However, in Fig. 11 the difference is greater. In the approximate, first order solution $E_{11} = a_{11}$, and hence this strain is independent of u_1' and u_2'. The approximate normalized axial stress simply falls along a straight line with the slope of the curve in Fig. 11 at $E_{11} = 0$. That the predictions in Fig. 11 depart from a single straight line is due entirely to higher order terms; this discrepancy has no effect on the prediction of kink band angle and compressive strength. At the end of this section further comparisons are made between exact and appropriate solutions which do relate to these predictions. It should be added that the relative error between exact and approximate solutions for T_{22}^p and T_{12}^p is comparable to that in Fig. 11 if the third order terms, $-\sigma\phi^2$ and $T_{22}\phi$, in eqn (82) are omitted. For example, without $-\sigma\phi^2$ the normal stress vanishes when $\beta = 0$, rather than being compressive as shown in Fig. 12; the discrepancy is about the same for $\beta > 0$.

The curves in Figs 10–13 for $\beta = 18°$ and $20°$ have both continuous and dotted portions. The dotted portion starts where matrix failure (cracking parallel to the fibers) initiates; this portion is predicted without modifying the theoretical model to account for cracks. (All curves, including the dotted portions, end when $S_r = 0.066$, which is the limiting value used in Section 2.) The local fracture event is estimated from average ultimate tensile strengths of unidirectional specimens with fiber angles of 30°, 45° and 90° (Schapery, 1989). Specifically, the fracture criterion is

$$T_{22}^p = \sigma_{90} - 0.28T_{12}^p \tag{83}$$

where $\sigma_{90} \simeq 10$ ksi is the average strength of 90° coupons; this criterion fits the data with an error of less than 7%. The ratio of normal-to-shear stress at which matrix failure is predicted in the band is bracketed by that for the $\theta = 30°$ and 45° unidirectional specimens. The use of eqn. (83) in the band analysis neglects the effects of axial fiber strain and through-the-thickness strain. There is also a size effect. A limited size effect study was made by O'Brien and Salpekar (1992), who studied unidirectional carbon/epoxy coupons in tension and three point bending with stress normal to the fibers. Typical kink bands involve a much smaller volume of material than that in the tensile specimens employed. Strengths from three point bending specimens are believed to provide a more realistic strength for our purposes. From the reported data we estimate a local transverse strength of our composite of $\sigma_{90} = 14$ ksi, and have used this value in eqn (83) for the predictions in Figs 10–13. Clearly, better understanding and data on the local strength than now exists are needed; but, in the absence of better information, we shall use the proposed failure criterion in discussing kink band initiation. (In the subsequent analysis an experimentally acceptable

kink band angle of 17° is predicted if $\sigma_{90} = 14$ ksi, whereas an unacceptably low value of 11° is predicted if $\sigma_{90} = 10$ ksi.) It should be added that others have used a Weibull-based theory for estimating strength of fiber composites of different volumes. However, it is doubtful that this theory is valid for estimating transverse strength in small fiber misalignment bands as it does not account for the effect of the ratio of fiber diameter-to-band width; it is likely that the Weibull scaling rule over-predicts this local strength.

Prediction of kink band angle and compressive strength

Let us now interpret the results in Fig. 10 for predicting kink band angle and compressive strength. For this purpose we suppose that the composite contains many different slender bands of wavy fibers, each with a different value of β and θ_0. As in tensile fracture of brittle materials, we are interested in identifying the critical band, i.e. that imperfection band which develops into a local kink band and then propagates. According to Fig. 10, the $\beta = 0$ band is the first one to buckle, i.e. as the axial stress is increased, u_2' grows more rapidly than that for $\beta > 0$ and becomes unbounded at the maximum in the curve. However, this prediction is for a long, unconstrained band. In reality, the axial stress will be higher than shown for a given local u_2' because of the constraining effect of the adjacent material at the ends of the band. The same will be true for $\beta > 0$ until cracks develop parallel to the fibers (cf. Fig. 2). When this happens there is a loss in shear stiffness. In addition, the effective value of E_2 decreases. Referring to eqn (73) for the case $\tau^\circ_{12} = \sigma^\circ_2 = 0$, if $E_2 \simeq 0$ and G_{12} is reduced due to the cracks, the axial stress for a given u_2' will be less than that for $\beta = 0$ without cracks. If this happens for values of u_2' beyond the predicted maximum stress point then immediate buckling of a slender band is expected. This type of local failure is predicted first for $\beta = 17°$, although only 2° intervals for β are shown in Fig. 10. The constraining effect prior to cracking in bands with smaller values of β is assumed great enough that the axial buckling stress for these bands is larger than that which causes cracking in the $\beta = 17°$ band. Of course, for a sufficiently long band with $\beta < 17°$, local buckling may occur without matrix cracking. However, considering the work needed for kink band growth, the propagation of this buckled band is not expected to occur as readily as one with matrix cracks.

The value of S_r at which matrix cracking is predicted is found to be practically the same as that for which the stress in Figs 5 and 7 is maximum. Thus, an accurate representation of material behavior in the neighborhood of the maximum stress is needed for predicting the kink band angle if it depends on the development of matrix cracks.

After the matrix cracks and a segment of a band of wavy fibers buckles, propagation as a kink band is expected to occur because of the large fiber rotations induced by local buckling. Referring to Fig. 2, if one imagines that very large shearing strains develop over some length $\leqslant L$, the fibers just *outside* of the initial band (but within $z^2 = W^2$) will rotate. The effect of this rotation may be the same as increasing ϕ_0 in a one-dimensional band analysis, so that the compressive stress needed for kink band propagation may be considerably below that required for initiation (cf. Fig. 14). Kyriakides *et al.* (1995) found experimentally that the axial stress for propagation is approximately 80% of the initiation value.

With these ideas in mind, it is suggested that the kink band angle is the smallest band angle for which cracking parallel to the fibers occurs, and that the maximum stress for this kink band angle provides a conservative estimate of the compressive strength. Unless $L \gg W$, the actual strength will be above this value because of constraint effects prior to cracking; this same argument provides another possible reason that the propagation stress is less than that required for kink band initiation.

Another issue concerns the width of a fully developed kink band, which is not necessarily the same as the initial band width W. According to the one-dimensional analysis, as the compressive loading is increased from zero, the largest $\phi_0(z)$ within a given band leads to the largest u_2', at any given axial stress. The shearing strain therefore gradually becomes more concentrated where ϕ_0 is maximum. As this localization develops, fiber bending stresses increase and eventually cause fiber fracture. As discussed in the Introduction, both

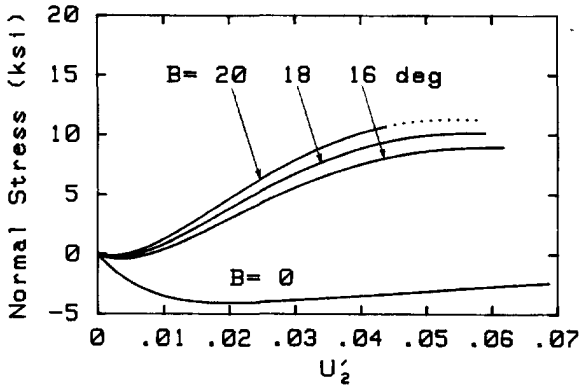

Fig. 15. True stress T'_{22} normal to the current fiber direction for $a_{22} = 0$.

one- and two-dimensional analyses predict realistic kink band widths from the spacing of the maximum moments.

Additional results

Many additional cases have been studied. Here we shall summarize the primary findings. The effect of the initial fiber angle ϕ_0 on the kink band angle was investigated, and it was found that the effect is relatively small. As examples, for a realistic range in which $\phi_0 = 1°$, $2°$, and $3°$, then $\beta = 16°$, $17°$ and $18°$, respectively.

A cross-ply laminate consists of plies with mutually perpendicular fiber orientations. Let us suppose the lay-up is symmetric across the mid-plane, and a uniaxial compressive load is applied in one of the average fiber directions. The compressive strength of 0° plies will be affected by the 90° plies in the laminate because these latter plies constrain the deformation normal to the loading. For a carbon/epoxy laminate with, for example, an equal number of 0° and 90° plies, the transverse strain a_{22} in the 0° plies is practically zero. Figures 10–14 are for the case in which the overall transverse stress vanishes. If instead we specify that $a_{22} = 0$, then this stress is compressive. Figure 15 shows the resulting stress normal to the fibers; when compared to Fig. 12 the effect of the lateral compression is evident. It increases the kink band angle by 2.5°, so that it is 19.5° for this case. A 13% increase in compressive strength is predicted for the 0° plies; this latter result is consistent with Daniel's (1994) experimental findings in which the compressive strength of the 0° plies within a cross-ply laminate has been found to be roughly 10% higher than that of a unidirectional laminate.

It was mentioned earlier in this section that the approximate solutions developed in Section 4 agree closely with the numerical results presented so far. Referring to eqns (73) and (82) it is seen that the modulus E_1 does not appear, which stems from the assumption that $\alpha \equiv G_{12}(0)/E_1 \ll 1$. For the carbon/epoxy composite $\alpha \simeq 0.044$. On the other hand for a glass/epoxy composite with a relatively small fiber volume fraction of 0.45, Scotchply 1002 (Tsai and Hahn, 1980), we find $\alpha = 0.11$. For comparison purposes, this material was modeled simply by using the same nonlinear material functions as used for the carbon/epoxy composite but scaling them so that the initial values (at $S = 0$) agree with values measured for Scotchply. Figures 16 and 17 show exact and approximate results for the carbon/epoxy composite and Figs 18 and 19 for the hypothetical glass/epoxy composite. Agreement between the exact and approximate solutions is nearly as good for glass/epoxy as for carbon/epoxy. High values of β are included here to show how the discrepancy increases with increasing β, which is primarily due to geometric nonlinearities. Although the value of α is not zero, essentially the same discrepancy as in Figs 16 and 17 was found with vanishingly small values. Specifically, for a composite with inextensible fibers ($\alpha = 0$), both exact and approximate maxima in axial and normal stresses are approximately 4% and 2%, respectively, above those for the exact α if $\beta = 40°$; the increase is less for smaller β. This slight increase is essentially due to σ_1 in eqn (22) for plane strain. Kink band angles

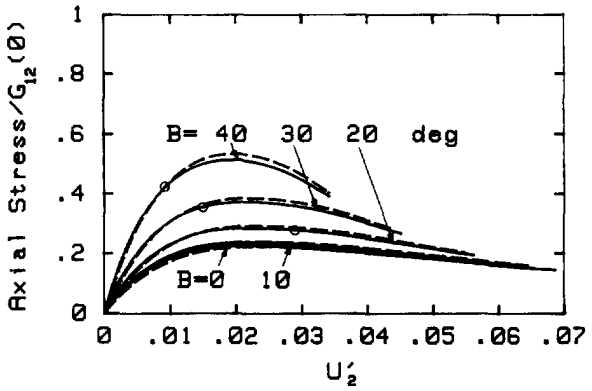

Fig. 16. Normalized axial stress. The solid lines are exact solutions and the dashed lines are approximate solutions [eqn (73)]. The points marked with O indicate when matrix cracking starts using eqn (83) and $\sigma_{90} = 14$ ksi.

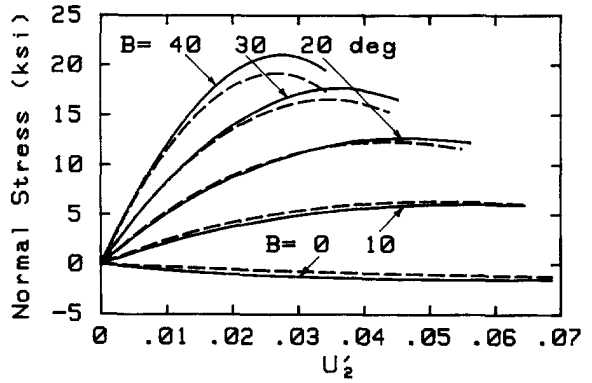

Fig. 17. True stress T_{22}^0 normal to the current fiber direction. The solid lines are exact solutions and the dashed lines are approximate solutions [eqn (82b)].

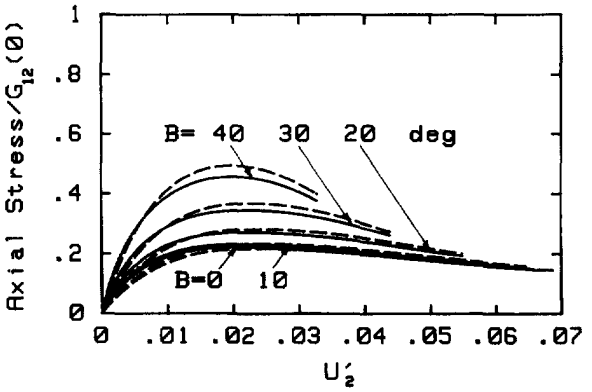

Fig. 18. Normalized axial stress for a hypothetical glass/epoxy composite. The solid lines are exact solutions and the dashed lines are approximate solutions [eqn (73)].

for some composites have been reported to exceed 30° (Hahn and Williams, 1986), and thus solutions for the range shown are practically relevant.

Observe that the stress for matrix crack initiation is marked in Fig. 16 with O. As with the smaller values of β in Fig. 10, this stress is seen to be an increasing function of β. Such behavior exists for all $\beta < 90°$, which supports the previously stated hypothesis that the kink band angle is the *smallest* β for which matrix cracking is predicted. It is also of interest to recall that most experimentally observed kink band angles do not exceed 30°. In this range Fig. 16 shows that matrix cracking does not develop until the axial stress is high

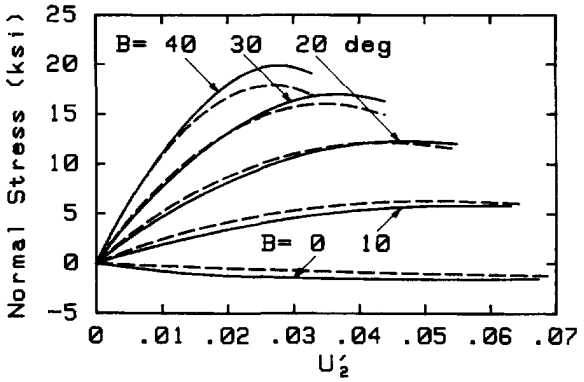

Fig. 19. True stress $T^{\prime}_{22}$ normal to the current fiber direction for a hypothetical glass/epoxy composite. The solid lines are exact solutions and the dashed lines are approximate solutions [eqn (82b)].

enough to cause microbuckling; only for $\beta > 30^{\circ}$ is matrix cracking predicted at stresses noticeably below the maximum stress.

All of the results discussed so far are for *plane strain*. A better idealization for in-plane kink bands is generalized plane stress if the composite is subjected only to in-plane loading. For this state, the thickness strain ε_3 is the same throughout the composite, but its value is not zero. Instead, it is calculated by specifying that $\sigma_3 = 0$ outside of the band. For all of the cases studied it was found that the plane strain results and generalized plane stress results are graphically indistinguishable. This agreement is a direct result of the smallness of ν_{21} ($\leqslant 0.025$).

When a band of wavy fibers is at a free surface (x_3 = constant) it could be expected that local buckling will occur more readily than predicted for plane strain. A simple way of estimating the effect of the free surface is to compare the earlier results in Figs 10 and 12 with those for plane stress. Plane stress results are similar to those in these figures, except the stresses are lower for each band angle; for example, if $\beta = 20^{\circ}$, then the reduction is 4% for σ_1 and 25% for $T^{\prime}_{22}$. As a result of the reduction in $T^{\prime}_{22}$ the kink band angle is increased from 17° to 22.5°. For this latter angle, the compressive strength is predicted to be 8% *higher* than that for plane strain. Tentatively, this result is taken to mean that kink bands will form more readily when the initial band of waviness is not along a surface, and hence that plane strain, rather than plane stress, is the more appropriate idealization. This conclusion is based on the assumption that a kink band does not originate at a stress concentration, such as at a hole or notch.

It is of interest to compare these last predictions to experimental results for a carbon/epoxy composite reported by Sutcliffe and Fleck (1994). They studied kink bands that were initiated from a through-thickness notch. Out-of-plane kink bands with $\beta \simeq 30^{\circ}$ were found, while for in-plane kink bands $\beta \simeq 25^{\circ}$. In the former case the band initiated along the notch tip, i.e. a free surface, with local deformation parallel to this free surface. In the latter case the deformation is in-plane, corresponding to the plane strain problem. This finding supports the prediction for our composite that β for plane stress is 5.5° greater than for plane strain.

There is another type of free surface effect which may be important. This type is concerned with a band of wavy fibers that intersects a surface x_2 = constant; i.e. when the initial band extends to the top or bottom edge of the geometry in Fig. 2. In this case formation of one internal matrix crack close to the surface may be sufficient to trigger local buckling and kink band formation. A case may be made that initial fiber waviness will exist in bands close to a free surface. Specifically, as noted in the Introduction, Budiansky (1983) used linear elastic analysis to argue that "localized deviations from ideal fiber alignment (e.g. due to inclusions, voids, fiber spacing irregularities) having no particular geometrical bias *induce* patterns of angular misalignment due to elastic distortion that arrange themselves into inclined domains. These rotations then induce plastic kinking into similarly inclined kink bands." He estimated the likely range of angles for these induced patterns to

be $10^\circ < \beta < 35^\circ$. Hence, to the extent that elastic deformation induced waviness may be treated as initial waviness in a nonlinear analysis, the present analysis predicts which of the bands is most likely to buckle. However, additional analysis is needed to determine an *effective* value of ϕ_0.

6. CONCLUDING REMARKS

This study served to illustrate the use of a recently developed constitutive theory for inelastic fiber composites and to provide a basis for predicting the kink band angle and compressive strength when the failure mechanism is microbuckling. The proposed mechanism of kink band initiation involves both matrix cracking and shear buckling in a band of initially misaligned fibers. The kink band angle is quite sensitive to the transverse strength of the composite and the stress normal to the fibers; prediction of this stress requires a good characterization of material nonlinearity under high shearing and normal stresses. However, the axial compressive strength is a relatively weak function of the kink band angle.

Strictly speaking, the initial fiber misalignment is assumed here to exist in long, slender bands with no significant variation of the misalignment angle along the length of the band. An additional assumption is that the wavelength of the initial fiber waviness is very long compared to fiber diameter and spacing. As noted in the Introduction, these assumptions have been removed in a two-dimensional numerical study by Kyriakides *et al.* (1995), which provides considerable additional insight into the initiation of kink bands through strain localization. An extension of their analysis, in which initial fiber waviness is generalized (such as discussed in the Introduction) and matrix cracking (at least its initiation, if not its growth) is accounted for should provide considerable additional understanding. Although the present one-dimensional analysis appears to capture the essential features of the compressive strength problem in view of the agreement with existing experimental results, it does not provide a theoretical basis for selecting an *effective* initial misalignment angle. By comparing results from the one- and extended two-dimensional analyses, it may be possible to develop a rule to calibrate the former one so that practical compressive strength predictions can be made in terms of realistic initial waviness. Alternatively, from selected uniaxial compression tests for strength and kink band angle, one could use the one-dimensional theory to calculate the effective ϕ_0 and local, transverse strength σ_{90}. Then, with this information, and assuming microbuckling-controlled failure, one could predict the compressive strength of laminates having plies with multiple fiber orientations and with other complexities, such as viscoelastic effects and complex thermomechanical loading histories. However, additional theoretical and experimental studies are needed to establish the range of validity of these approaches.

The present study has concentrated on mechanical response in the nonlinear, time independent range of behavior. However there are problems for which linear analysis should provide useful information. Consider, for example, a viscoelastic composite which is subjected to a low level of constant or cyclic loading over a long period of time. Linear theory may be adequate for predicting the growth of imperfections, which are then treated as initial imperfections in a residual strength analysis using nonlinear viscoelasticity theory. The equation based on simple shearing deformation given in the Introduction has been used to predict the growth of an initial misalignment imperfection in the linear viscoelastic range and its effect on residual strength following constant and cyclic loading (Schapery, 1992, 1993a,b). Slaughter and Fleck (1993) studied linear viscoelastic effects under constant axial stress, but they allowed for $\beta > 0$.

Finally, we observe that in the linear range one may represent an arbitrary fiber misalignment distribution and the resulting mechanical response by superposition of one-dimensional functions of z, each associated with a different band orientation β. This observation was made by Biot (1965) and used in his two-dimensional analysis of internal instabilities. It enables existing analyses of single deformation bands to be immediately extended to arbitrary initial fiber waviness by superposition. Although the nonlinear problem does not allow for superposition of solutions, it may be helpful to represent the initial

fiber waviness by a series of functions of z since each one alone leads to a solution that appears to contain the essential characteristics of the complete solution.

Acknowledgements—Sponsorship of this work by the Office of Naval Research, Solid Mechanics Program, with Dr Y. D. S. Rajapakse as scientific officer, is gratefully acknowledged. The author is indebted to Professor Kyriakides of the University of Texas at Austin and to Professor Daniel of Northwestern University for helpful discussions and for providing the pictures of kink bands in Fig. 1.

REFERENCES

Argon, A. S. (1972). Fracture of composites. In *Treatise on Materials Science and Technology* (Edited by H. Herman), Vol. 1, pp. 79–114. Academic Press, New York.

Biot, M. A. (1965). *Mechanics of Incremental Deformations*. Wiley, New York.

Budiansky, B. (1983). Micromechanics. *Computers Struc.* **16,** 3–12.

Budiansky, B. and Fleck, N. A. (1993). Compressive failure of fiber composites. *J. Mech. Phys. Solids* **41,** 183–211.

Daniel, I. M. (1993). Processing and compressive behavior of thick composites. In *Mechanics of Thick Composites* (Edited by Y. D. S. Rajapakse), Vol. 162, pp. 107–126., ASME AMD, New York.

Daniel, I. M. (1994). Private communication.

Fleck, N. A., Deng, L. and Budiansky, B. (1993). Prediction of kink width in fiber composites. Report MECH-203, Harvard University.

Fung, Y. C. (1965). *Fundamentals of Solid Mechanics*. Prentice-Hall, Englewood Cliffs, NJ.

Greszczuk, L. B. (1975). Microbuckling failure of circular fiber-reinforced composites, *AIAA J.* **13,** 1311–1318.

Hahn, H. T. and Williams, J. G. (1986). Compression failure mechanisms in unidirectional composites. In *Composite Materials* (7th Conference) (Edited by J. M. Whitney) ASTM STP 893, pp. 115–139. ASTM, PA.

Jones, R. M. (1975). *Mechanics of Composite Materials*. Hemisphere, New York.

Kyriakides, S., Arseculeratne, R., Perry, E. J. and Liechti, K. M. (1995). On the compressive failure of fiber reinforced composites. *Int. J. Solids Structures* **32,** 689–738.

Lamborn, M. J. and Schapery, R. A. (1993). An investigation of the existence of a work potential for fiber-reinforced plastic. *J. Compos. Mater.* **27,** 352–382.

Lou, Y. C. and Schapery, R. A. (1971). Viscoelastic characterization of a nonlinear fiber-reinforced plastic. *J. Compos. Mater.* **5,** 208–234.

Mignery, L. A. and Schapery, R. A. (1991). Viscoelastic and nonlinear adherend effects in bonded composite joints. *J. Adhesion* **34,** 17–40.

O'Brien, T. K. and Salpekar, S. A. (1992). Scale effects on the transverse tensile strength of graphite epoxy composites. NASA Technical Memorandum 107637, Langley Research Center, Hampton, VA.

Rosen, B. W. (1965). Mechanics of composite strengthening. In *Composite Materials*, pp. 37–75. American Society of Metals, Metals Park, OH.

Schapery, R. A. (1989). Mechanical characterization and analysis of inelastic composite laminates with growing damage. In *Mechanics of Composite Materials and Structures* (Edited by J. N. Reddy and T. L. Teply), Vol. 100, pp. 1–9. ASME AMD, New York.

Schapery, R. A. (1990). A theory of mechanical behavior of elastic media with growing damage and other changes in structure. *J. Mech. Phys. Solids* **38,** 215–253.

Schapery, R. A. (1992). Analysis of local buckling in viscoelastic composites. In *Local Mechanics Concepts for Composite Material Systems* (Edited by J. N. Reddy and K. L. Reifsnider), pp. 229–250. Springer-Verlag, New York.

Schapery, R. A. (1993a). Nonlinear viscoelastic effects in the compressive behavior of fiber composites. In *Mechanics of Thick Composites* (Edited by Y. D. S. Rajapakse), Vol. 162, pp. 81–90. ASME AMD, New York.

Schapery, R. A. (1993b). Compressive strength and failure time based on local buckling in viscoelastic composites. *Appl. Mech. Rev.* **46,** Part 2, S221–S228.

Sicking, D. L. (1992). Mechanical characterization of nonlinear laminated composites with transverse crack growth. Ph.D. Thesis, Texas A&M University, College Station, TX.

Slaughter, W. S. and Fleck, N. A. (1993). Viscoelastic microbuckling of fiber composites. *ASME J. Appl. Mech.* **60,** 802–806.

Slaughter, W. S., Fleck, N. A. and Budiansky, B. (1992). Compressive failure of fibre composites: the roles of multi-axial loading and creep. Report MECH-199, Harvard University.

Sun, C. T. and Chen, J. L. (1989). A simple flow rule for characterizing nonlinear material behavior of fiber composites. *J. Compos. Mater.* **23,** 1009–1020.

Sun, C. T. and Rui, Y. (1990). Orthotropic elasto-plastic behavior of AS4/PEEK thermo-plastic composite in compression. *Mech. Mater.* **10,** 117–125.

Sutcliffe, M. P. F. and Fleck, N. A. (1994). Microbuckle propagation in carbon fibre–epoxy composites. *Acta Metall. Mater.* **42,** 2219–2231.

Tsai, S. W. and Hahn, H. T. (1980). Introduction to composite materials. Technomic, Lancaster, PA.

Waas, A. M., Babcock, C. D. and Knauss, W. G. (1990). A mechanical model for elastic fiber microbuckling. *ASME J. Appl. Mech.* **57,** 138–149.